

Materials Science and Engineering A 412 (2005) 129-136



Characterization of reinforced concrete beams strengthened by steel reinforced polymer and grout (SRP and SRG) composites

B. Barton^a, E. Wobbe^b, L.R. Dharani^{a,*}, P. Silva^b, V. Birman^c, A. Nanni^b, T. Alkhrdaji^d, J. Thomas^d, G. Tunis^e

^a Department of Mechanical and Aerospace Engineering, University of Missouri-Rolla, Rolla, MO 65409-0050, USA
 ^b Department of Civil, Architectural and Environmental Engineering, University of Missouri-Rolla, Rolla, MO 65409-0030, USA
 ^c Engineering Education Center, University of Missouri-Rolla, One University Building, St. Louis, MO 63121, USA
 ^d Structural Group, 7455 New Ridge Road, Suite T, Hanover, MD 21076, USA
 ^e Hardwire, LLC, 1000 Quinn Avenue, Pocomoke City, MD 21851, USA

Received in revised form 16 May 2005

Abstract

The use of externally bonded steel reinforced polymer (SRP) and steel reinforced grout (SRG) is a promising new technology for increasing flexural, compressive, and shear capacities of reinforced concrete (RC) members. The flexural performance of RC beams with externally bonded SRP and SRG has been investigated experimentally using four-point bending. The material constants for single-ply SRP and SRG were experimentally determined from coupon tensile tests and torsion tests. Analytical models based on the first-order and higher-order shear deformation theories have been developed to predict the behavior of the retrofitted RC beams. Comparisons between the analytical models and the experimental results show a good correlation for the midspan deflection until the reinforcing steel reaches the plastic region.

© 2005 Elsevier B.V. All rights reserved.

Keywords: Composites; Steel reinforced polymer; Steel reinforced grout; Reinforced concrete; Shear deformation

1. Introduction

Problems associated with increases in load, structural degradation, or even structures reaching their life cycle in civil infrastructure have prompted the search for low-cost retrofitting materials and methods. Among the materials that are currently investigated are steel reinforced polymer (SRP) and steel reinforced grout (SRG). These materials are composed of high strength steel cords (readily available from the tire industry) embedded in a polymeric resin or cementitious grout. SRP and SRG can be applied using a wet lay-up technique similar to that of carbon or glass fiber reinforced polymers (FRP). Based on preliminary testing, SRP and SRG have shown great potential for strengthening RC beams.

Two analytical models of the analysis of SRP or SRG strengthened reinforced concrete beams are presented in this paper. Because typical reinforced concrete (RC) beams are thick

specimens, the effects of shear cannot be neglected when determining the beams response to various loading [1]. The first analytical model is based on the first-order shear deformation theory (FSDT), otherwise known as the Hencky–Mindlin plate theory [2,3]. The second model is based on a higher-order shear deformation theory (HSDT) [4,5]. Plasticity of the internal reinforcing steel affects the laminate extensional, coupling, and bending stiffnesses. The analytical response predicted by the models of RC beams externally strengthened with SRP and SRG subjected to four-point bending was compared to the experimental data. The results shown in the paper illustrate that standard theories of shear-deformable composite laminates are applicable to the analysis of the response of SRP and SRG strengthened RC beams.

2. Experimental procedure

2.1. RC beams

In order to investigate the response of RC beams with externally applied SRP and SRG, four 243.8 cm \times 27.9 cm \times 20.3 cm

Corresponding author. Tel.: +1 573 341 6504; fax: +1 573 341 4607. *E-mail address*: dharani@umr.edu (L.R. Dharani).

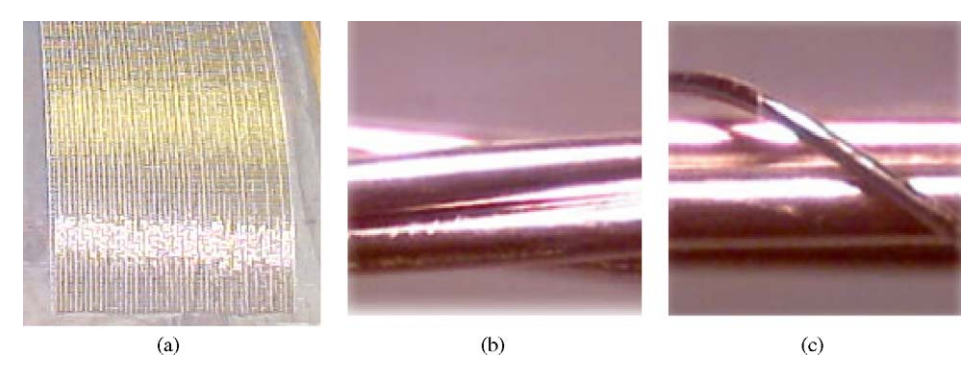


Fig. 1. Steel reinforcement: (a) steel tape, (b) 3X2 cord and (c) 3SX cord.

 $(8 \text{ ft} \times 11 \text{ in.} \times 8 \text{ in.})$ beams were cast with two #5 (15.9 mm) bars of internal tensile reinforcement and two #3 (9.5 mm) reinforcing bars on the compression side of the beam. The tension face of each beam where the SRP/SRG material was to be applied was mechanically roughened with a surface preparation grinder, swept clean, and then vacuumed so that all remaining particles were removed in order to obtain a proper bond.

The steel fabric used in the SRP and SRG was composed of unidirectional high strength steel cords with a scrim backing to maintain spacing and alignment (Fig. 1(a)). The steel fabric was cut into $203.2 \,\mathrm{cm} \times 15.2 \,\mathrm{cm}$ ($80 \,\mathrm{in.} \times 6 \,\mathrm{in.}$) sheets to be applied to the tension side of the beams. The width was recommended by the manufacturer to ensure that proper bonding occurs along the edge of the laminate. The HardwireTM (Hardwire, LLC, Pocomoke City, MD) high-density cord (23 cords per inch) type 3X2 (Fig. 1(b)) was applied to specimens SRP-1 and SRP-2 using Sikadur 330 (Sika Corporation, Lyndhurst, NJ) epoxy resin. As for specimens SRG-1 and SRG-2, SikaTop 121 (Sika Corporation, Lyndhurst, NJ) cementitious grout was used to apply the medium density (12 cords per inch) 3SX cord type (Fig. 1(c)). The medium density allows for the cement to pass through in order to create a stronger bond, and the cord geometry allows for better adhesion and mechanical lock between the grout and the steel cords [6]. Specimens SRP-1 and SRG-1 consisted of one ply of the material, while specimens SRP-2 and SRG-2 consisted of two plies.

Each of the four specimens were loaded in a four-point arrangement with a constant moment region of 71.1 cm (28 in.), and tested as a simply supported member with a span length of 213.4 cm (84 in.) (Fig. 2) [7]. During the testing of each beam, the midspan deflection, as well as the deflections under the point loads, was measured using a linear variable displacement transducer (LVDT). LVDTs were also used to determine if any settlement occurred at the supports. The load was measured using a 445 kN (100 kip) load cell. All data from the load cell and LVDTs was recorded through a data acquisition system at a scan rate of 3 Hz. During testing, loading was periodically paused in order to identify and mark crack formations and growth.

2.2. Coupon testing

Six concrete cylinders were cast according to ASTM standards and tested to determine the compressive strength at 28 days and at the time of testing. The yield strength of the internal reinforcing steel, σ_{ys} , was determined by performing a standard coupon tension test on three specimens, which produced an average strength of 436 MPa (63 ksi).

Tensile specimens were used to determine the material properties of the SRP and SRG lamina. Several specimen geometries were tried including strips, tabbed strips—as suggested by ASTM D 3039, and dog bone shaped specimens. Unidirectional longitudinal strips failed in the grips of the testing machines, while tabbed strips prematurely failed at the tab—lamina

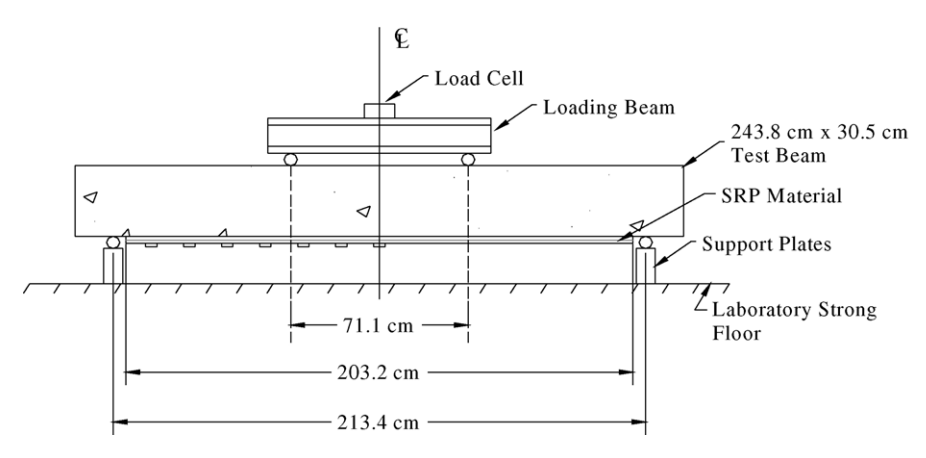


Fig. 2. Schematic representation of RC beam test setup.

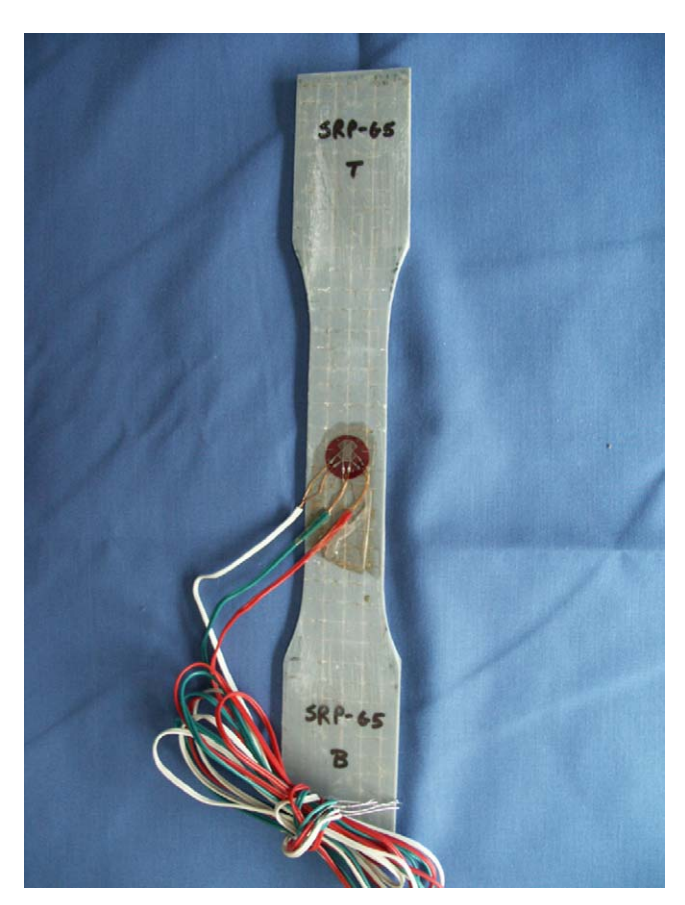


Fig. 3. SRP tensile specimen.

interface. Finally, the dog bone shaped geometry shown in Fig. 3 was chosen for the experimental study. In order to assure consistency and reduce stress concentrations in specimens, a mold was machined and used to produce the tensile specimens. The overall length of the specimens was 25 cm (10 in.) and the width of the gage section was 2.5 cm (1 in.). The specimens were subjected to uniaxial tension at a rate of 0.025 cm/min (0.01 in./min) and the stress–strain response was recorded via strain gages and verified via an extensometer at a scan rate of $10\,\mathrm{Hz}$. This specimen geometry produced repeatable results and failure in the gage section for both the longitudinal (E_1 and ν_{12}) and transverse (E_2 and ν_{21}) directions.

The method of determining the in-plane shear response described in ASTM D 3518 could not be applied to SRP since it requires a minimum of 16 plies (the average thickness of a SRP lamina is on the order of $0.25 \, \mathrm{cm} \, (0.10 \, \mathrm{in.})$). Therefore, hollow cylindrical tubes were constructed with the cords oriented along the longitudinal axis (Fig. 4) [8]. Circular end plugs with a central threaded hole were machined for each end of the cylindrical tube. To ensure proper alignment, the plugs were screwed on to a single piece of threaded rod and adhered to the inside of the tubes using Sikadur 330. Upon curing of the epoxy, the threaded rod was removed and a threaded stud was screwed into each of the end plugs. The specimen was then tested in pure torsion. Strain gage rosettes were used to determine the stress–strain behavior, and in turn, the shear modulus ($G_{12} = G_{13}$). Because of the difficulty in constructing hollow cylindrical tubes of

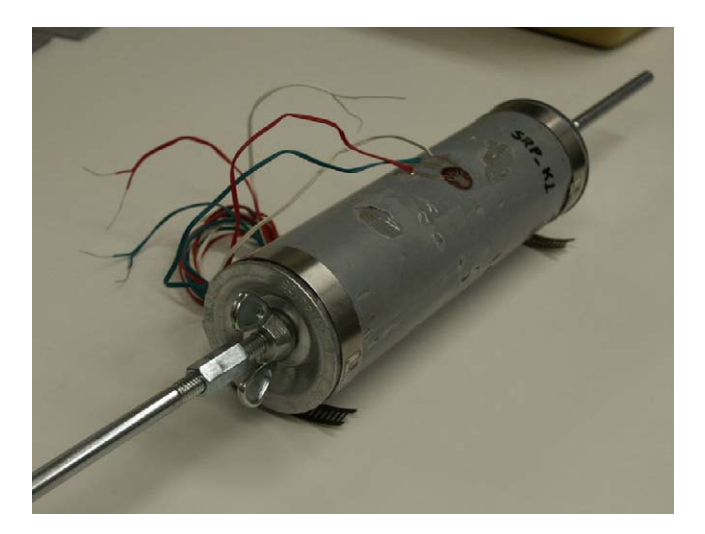


Fig. 4. SRP torsion specimen.

SRG, the shear modulus was estimated using the inverse rule of mixtures.

3. Analytical models

When the FSDT and HSDT are applied to laminate structures, it is typically assumed the individual lamina thicknesses are constant through the width. In order to accommodate this assumption, a "smeared beam" model of the RC beam is introduced replacing the actual cross-section (Fig. 5). The cross-section of the original beam has been smeared into five layers of the same width with the compression steel neglected. The thickness of each layer is determined by maintaining the same cross-sectional area as the material had in the original beam. Since the beam is not symmetric about the middle surface, coupling exists between the moments and in-plane forces.

Each layer is assumed linear-elastic, with the exception of the steel layer which is assumed linear-elastic up to the yield stress and then perfectly plastic after yielding. The tensile strength of concrete is neglected. The concrete and steel layers are treated as homogeneous isotropic materials characterized by two independent elastic constants, while the SRP/SRG layer is treated as a specially orthotropic material characterized by five independent elastic constants.

The models are used to predict the response of a RC beam reinforced with externally bonded SRP/SRG in four-point bending (Fig. 6). Due to the symmetry of both the beam and the loading it is only necessary to model half of the beam $(0 \le x \le L/2)$.

3.1. First-order shear deformation theory (FSDT) based model

The FSDT model is based upon the following displacement field [2] (standard notations are used throughout the paper):

$$u(x, y, z) = u_0(x, y) + z\psi_x(x, y)$$

$$v(x, y, z) = v_0(x, y) + z\psi_y(x, y)$$

$$w(x, y, z) = w_0(x, y)$$
(1)

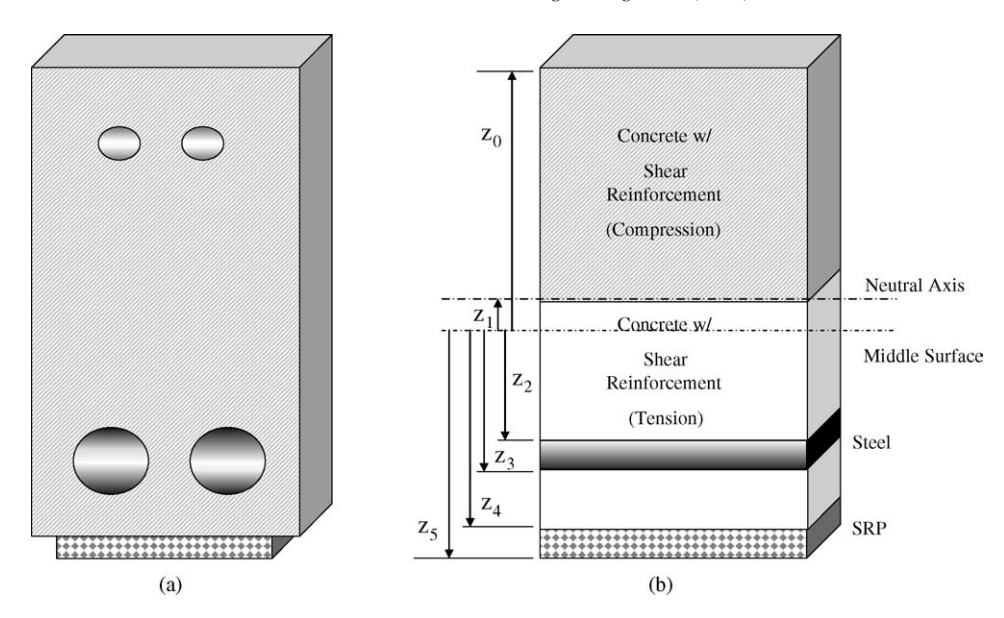


Fig. 5. Schematic representation of the cross-section of the modeled beam: (a) actual and (b) smeared cross-sections.

where u, v, and w are the displacement components in the x, y, and z directions, respectively; u_0 , v_0 , and w_0 the displacements of a point (x, y) on the midplane; ψ_x and ψ_y are the rotations of a normal to midplane about the y and x axes, respectively.

Assuming symmetry about the x–z plane, deflection and slopes in the y-direction will be symmetric and negligible. Therefore, the problem is two-dimensional. The in-plane stress resultant, N_x , the transverse shear stress resultant, Q_x , and resultant bending moment, M_x , at x can be evaluated as

$$N_{x} = \int_{-h/2}^{h/2} \sigma_{x} dz \qquad M_{x} = \int_{-h/2}^{h/2} z \sigma_{x} dz$$

$$Q_{x} = \int_{-h/2}^{h/2} \tau_{zx} dz \qquad (2)$$

where h is the total height of the beam. Concrete layers being incapable of carrying tensile loads, it is reasonable to assume the internal reinforcing steel and SRP/SRG layers are subjected to plane stress. Treating each layer as an orthotropic lamina, the stresses in terms of engineering strains are

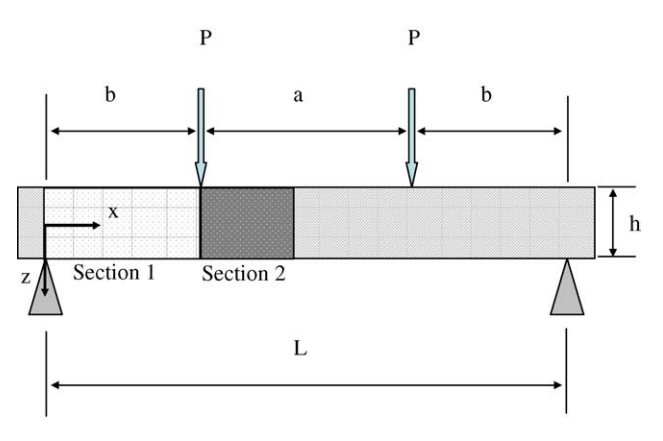


Fig. 6. Diagram of loading configuration.

given by

$$\left\{ \begin{array}{l}
 \sigma_{x} \\
 \sigma_{y} \\
 \tau_{xy}
 \end{array} \right\} = \begin{bmatrix}
 \bar{Q}_{11} & \bar{Q}_{12} & \bar{Q}_{16} \\
 \bar{Q}_{21} & \bar{Q}_{22} & \bar{Q}_{26} \\
 \bar{Q}_{16} & \bar{Q}_{26} & 2\bar{Q}_{66}
 \end{bmatrix} \left\{ \begin{array}{l}
 \varepsilon_{x} \\
 \varepsilon_{y} \\
 \gamma_{xy}
 \end{array} \right\}$$
(3)

where the \bar{Q}_{ij} are the components of the transformed lamina stiffness matrix. For isotropic materials, $\bar{Q}_{16}=0$ and $\bar{Q}_{66}=\bar{Q}_{55}=G_{12}$ (\bar{Q}_{55} is the stiffness in the x-z plane). When the x and y axes coincide with the principal axes of a specially orthotropic material, $\bar{Q}_{16}=0$. Inserting (3) into (2), and neglecting transverse displacements (i.e. $\varepsilon_y\approx 0$) yields the following formulas for the stress resultants and stress couples

$$N_{x} = \int_{z_{0}}^{z_{1}} \bar{Q}_{11_{csr}}(u_{0,x} + z\psi_{x,x}) dz$$

$$+ \int_{z_{2}}^{z_{3}} \bar{Q}_{11_{steel}}(u_{0,x} + z\psi_{x,x}) dz$$

$$+ \int_{z_{4}}^{z_{5}} \bar{Q}_{11_{SRP}}(u_{0,x} + z\psi_{x,x}) dz$$

$$M_{x} = \int_{z_{0}}^{z_{1}} z \bar{Q}_{11_{csr}}(u_{0,x} + z\psi_{x,x}) dz$$

$$+ \int_{z_{2}}^{z_{3}} z \bar{Q}_{11_{steel}}(u_{0,x} + z\psi_{x,x}) dz$$

$$+ \int_{z_{4}}^{z_{5}} z \bar{Q}_{11_{SRP}}(u_{0,x} + z\psi_{x,x}) dz$$

$$Q_{x} = \int_{z_{0}}^{z_{1}} \bar{Q}_{55_{csr}} \left(\psi_{x} + \frac{\partial w_{0}}{\partial x}\right) dz$$

$$+ \int_{z_{2}}^{z_{3}} \bar{Q}_{55_{steel}} \left(\psi_{x} + \frac{\partial w_{0}}{\partial x}\right) dz$$

$$+ \int_{z_{1}}^{z_{5}} \bar{Q}_{55_{SRP}} \left(\psi_{x} + \frac{\partial w_{0}}{\partial x}\right) dz$$

$$(4)$$

where the subscript "csr" represents the compressive concrete with shear reinforcement layer. Eq. (4) is written by assumption that concrete cannot resist tensile stresses.

The equations of equilibrium become

$$\begin{bmatrix} A & B \\ B & D \end{bmatrix} \begin{Bmatrix} u_{0,x} \\ \psi_{x,x} \end{Bmatrix} = \begin{Bmatrix} N_x \\ M_x \end{Bmatrix} \qquad A_{55} \left(\psi_x + \frac{\partial w_0}{\partial x} \right) = Q_x$$
(5)

where A, B, and D are the laminate extensional, coupling, and bending stiffnesses, respectively, given by

$$A = \bar{Q}_{11_{\text{csr}}}(z_1 - z_0) + \bar{Q}_{11_{\text{steel}}}(z_3 - z_2) + \bar{Q}_{11_{\text{SRP}}}(z_5 - z_4)$$

$$B = \frac{1}{2}[\bar{Q}_{11_{\text{csr}}}(z_1^2 - z_0^2) + \bar{Q}_{11_{\text{steel}}}(z_3^2 - z_2^2) + \bar{Q}_{11_{\text{SRP}}}(z_5^4 - z_4^2)]$$

$$D = \frac{1}{3}[\bar{Q}_{11_{\text{csr}}}(z_1^3 - z_0^3) + \bar{Q}_{11_{\text{steel}}}(z_3^3 - z_2^3) + \bar{Q}_{11_{\text{SRP}}}(z_5^3 - z_4^3)]$$

$$A_{55} = k[\bar{Q}_{55_{\text{csr}}}(z_1 - z_0) + \bar{Q}_{55_{\text{steel}}}(z_3 - z_2) + \bar{Q}_{55_{\text{SRP}}}(z_5 - z_4)]$$
(6)

In (6), k is the shear correction factor taken to be 5/6. Eq. (5) can be solved in a closed-form by considering two sections of the beam, i.e. section 1: (0 < x < b) where the moment increases linearly $\{N_x = 0, M_x = Px/w_{\text{beam}}, Q_x = P/w_{\text{beam}}\}$ and section 2: (b < x < L/2) where the moment is constant $\{N_x = 0, M_x = Pb/w_{\text{beam}}, Q_x = 0\}$, w_{beam} , being the width of the beam. Once $u_{0,x}$ and $\psi_{x,x}$ have been evaluated, they can be integrated with respect to x. Applying the boundary and junction conditions:

$$w|_{x=0} = 0 M_x|_{x=0} = 0 u^{(1)}|_{x=b} = u^{(2)}|_{x=b}$$

$$\psi_x^{(1)}|_{x=b} = \psi_x^{(2)}|_{x=b} w^{(1)}|_{x=b} = w^{(2)}|_{x=b}$$

$$\psi_x|_{x=L/2} = 0 u_0|_{x=L/2} = 0 (7)$$

where the superscripts 1 or 2 represent the section, the closedform solution for the deflection is given as

$$w_{0} = \begin{cases} \frac{Px}{w_{\text{beam}}A_{55}} - \frac{APx^{3} + 3APb(b - L)x}{6w_{\text{beam}}(AD - B^{2})} & \text{for } 0 < x < b, \\ \frac{Pb}{w_{\text{beam}}A_{55}} - \frac{APb^{3} + 3APb(x - L)x}{6w_{\text{beam}}(AD - B^{2})} & \text{for } b \le x < \frac{L}{2} \end{cases}$$
(8)

where b is the distance from the support to the applied load.

The proceeding analysis was based on the assumption that each layer is linear elastic. When the internal reinforcing steel yields, Eq. (3) becomes invalid for this layer. Treating the internal steel as elastic perfectly plastic, upon the onset of yielding the in-plane stress resultant and resultant bending moment of Eq. (4) are replaced with

$$N_{x} = \int_{z_{0}}^{z_{1}} \bar{Q}_{11_{\text{csr}}}(u_{0,x} + z\psi_{x,x}) \,dz + \int_{z_{2}}^{z_{3}} \sigma_{ys} \,dz$$

$$+ \int_{z_{4}}^{z_{5}} \bar{Q}_{11_{\text{SRP}}}(u_{0,x} + z\psi_{x,x}) \,dz$$

$$M_{x} = \int_{z_{0}}^{z_{1}} z \bar{Q}_{11_{\text{csr}}}(u_{0,x} + z\psi_{x,x}) \,dz + \int_{z_{2}}^{z_{3}} z \sigma_{ys} \,dz$$

$$+ \int_{z_{0}}^{z_{5}} z \bar{Q}_{11_{\text{SRP}}}(u_{0,x} + z\psi_{x,x}) \,dz$$

$$(9)$$

where σ_{ys} is the yield stress of the internal reinforcing steel. Introducing,

$$A_{R} = \bar{Q}_{11_{csr}}(z_{1} - z_{0}) + \bar{Q}_{11_{SRP}}(z_{5} - z_{4})$$

$$N_{ys} = \sigma_{ys}(z_{3} - z_{2})$$

$$B_{R} = \frac{1}{2}[\bar{Q}_{11_{csr}}(z_{1}^{2} - z_{0}^{2}) + \bar{Q}_{11_{SRP}}(z_{5}^{2} - z_{4}^{2})]$$

$$M_{ys} = \frac{1}{2}\sigma_{ys}(z_{3}^{2} - z_{2}^{2})$$

$$D_{R} = \frac{1}{3}[\bar{Q}_{11_{csr}}(z_{1}^{3} - z_{0}^{3}) + \bar{Q}_{11_{SRP}}(z_{5}^{3} - z_{4}^{3})]$$
(10)

the equations of equilibrium become,

$$\begin{bmatrix} A_{R} & B_{R} \\ B_{R} & D_{R} \end{bmatrix} \begin{Bmatrix} u_{0,x} \\ \psi_{x,x} \end{Bmatrix} + \begin{Bmatrix} N_{ys} \\ M_{ys} \end{Bmatrix} = \begin{Bmatrix} N_{x} \\ M_{x} \end{Bmatrix}$$
(11)

where the loading terms on the right-hand side remain the same as those used previously for the elastic case.

Since the steel layer does not yield along the entire length of the beam at the same load, the neutral axis varies along the length of the beam after the onset of yielding. Because of this phenomenon, it is necessary to subdivide the beam along the *x*-direction into smaller elements and evaluate the reduced stiffnesses for each element. The solution can then be obtained using an iterative approach.

3.2. Higher-order shear deformation theory (HSDT) based model

The HSDT model is based on the following displacement field [4]:

$$u(x, y, z) = u_0(x, y) + z\psi_x(x, y) + z^3\phi_x(x, y)$$

$$v(x, y, z) = v_0(x, y) + z\psi_y(x, y) + z^3\phi_y(x, y)$$

$$w(x, y, z) = w_0(x, y)$$
(12)

The terms associated with z^2 are equal to zero as a result of the requirement of zero shear stresses on the upper and lower surfaces [4]. By imposing the boundary condition for the shear strain, γ_{xz} , to be zero on the outer surfaces, it can be shown that

$$\phi_x = -\left(\frac{4}{3h^2}\right)(\psi_x + w_{,x})\tag{13}$$

The transverse shear stress resultant is given by

$$Q_x = S_{55}(\psi_x + w_{,x}) \tag{14}$$

where

$$S_{55} = \int_{-h/2}^{h/2} \left[1 - \left(\frac{2z}{h} \right)^2 \right] \bar{Q}_{55} \, \mathrm{d}z \tag{15}$$

Since the transverse shear stress resultant is independent of *x* in both sections 1 and 2

$$\frac{\partial Q_x}{\partial x} = 0 \tag{16}$$

so that

$$\psi_{x,x} = -w_{,xx} \tag{17}$$

Combining (17) with the equations of equilibrium results in

$$\begin{bmatrix} A & -B \\ B & -D \end{bmatrix} \begin{Bmatrix} u_{0,x} \\ w_{,xx} \end{Bmatrix} = \begin{Bmatrix} N_x \\ M_x \end{Bmatrix}$$
(18)

prior to the yielding of steel, and

$$\begin{bmatrix} A_{R} & -B_{R} \\ B_{R} & -D_{R} \end{bmatrix} \begin{Bmatrix} u_{0,x} \\ w_{,xx} \end{Bmatrix} + \begin{Bmatrix} N_{ys} \\ M_{ys} \end{Bmatrix} = \begin{Bmatrix} N_{x} \\ M_{x} \end{Bmatrix}$$
(19)

subsequent to the steel yielding. The problem can then be solved following the same approach as that used for the FSDT. The closed-form solution for the deflection prior to the yielding of the internal reinforcing steel is

$$w_{0} = \begin{cases} \frac{Px}{w_{\text{beam}} S_{55}} - \frac{APx^{3} + 3APb(b-L)x}{6w_{\text{beam}}(AD - B^{2})} & \text{for } 0 < x < b, \\ \frac{Pb}{w_{\text{beam}} S_{55}} - \frac{APb^{3} + 3APb(x-L)x}{6w_{\text{beam}}(AD - B^{2})} & \text{for } b \le x < \frac{L}{2} \end{cases}$$
(20)

When the solution based on the FSDT (8) is compared with that obtained using the HSDT (20), it can be seen that the only difference in expressions for deflection is related to the terms A_{55} and S_{55} .

4. Numerical results and comparison with experimental data

The properties of both SRP and SRG materials are summarized in Table 1.

Notably, experimentally obtained values of the minor Poisson's ratio v_{21} for SRP and SRG are close to zero, with SRPs being slightly negative. These values violate the equation that

SRP and SRG lamina properties

	SRP ($v_f = 16\%$)	SRG ($\nu_f = 6.5\%$)
Longitudinal modulus, E_1	27.0 GPa (5160 ksi)	14.6 GPa (2120 ksi)
Transverse modulus, E_2	5.86 GPa (850 ksi)	3.45 GPa (500 ksi)
Shear modulus, G_{12} and G_{13}	3.03 GPa (440 ksi)	2.07 GPa (300 ksi)
Major Poisson's ratio, ν_{12}	0.32	0.35
Minor Poisson's ratio, ν_{21}	-0.026	0

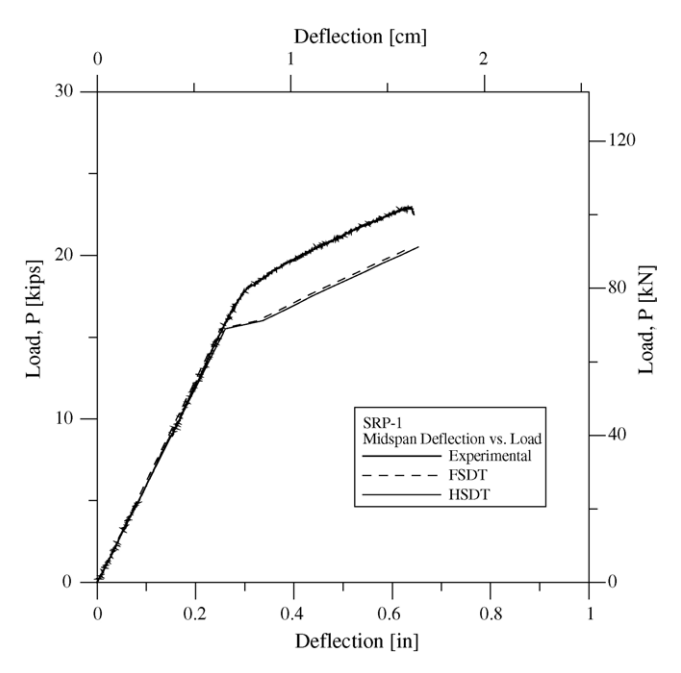


Fig. 7. Midspan deflection of SRP-1.

relates the Poisson's ratios to the modulus of elasticity for orthotropic materials [8],

$$\frac{\nu_{12}}{E_1} = \frac{\nu_{21}}{E_2} \tag{21}$$

A possible explanation to the difference between experimental and theoretical predictions for the minor Poisson ratio may be related to cracking of SRP and SRG subject to straining in the direction perpendicular to the reinforcements. Experimental results in Table 1 are in agreement with other studies of cord composites in which the minor Poisson's ratio of such materials was generally taken to be zero [9,10]. It should be noted that the value of the minor Poisson ratio has little effect on the numerical results obtained in this study.

The midspan deflection versus load plots for the four beam specimens are shown in Figs. 7–10. The experimental data from all four tests exhibit a linear initial region corresponding to elastic stresses in the reinforcing steel. Both the FSDT and HSDT models correlate well to the experimental values of the midspan deflection within this region.

A clearly defined yield point exists in both beams reinforced with SRP (SRP-1 and SRP-2), as can be seen in Figs. 7 and 8. The models predict yielding at a lower load than that observed in the experiments. It is likely that the difference in yield points is due to the scatter in the experimental yield stress for steel.

The two beams reinforced with SRG (SRG-1 and SRG-2), also exhibit an initial linear region (Figs. 9 and 10) that was accurately predicted by analytical models. The load–displacement plots for RC beams reinforced with SRG, Figs. 9 and 10, show small unloading–loading steps prior to yielding. This inconsistency in the load–displacement behavior could be attributed to interruptions of the tests to mark cracks or slight shifting of the LVDT due to concrete and/or matrix cracking. This behavior

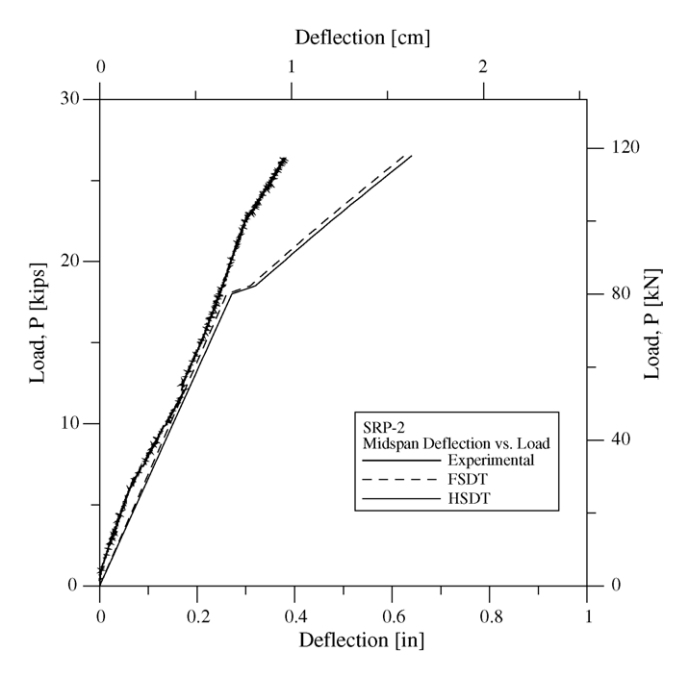


Fig. 8. Midspan deflection of SRP-2.

is not observed in the beams reinforced with SRP because the epoxy matrix has a much higher elongation at break than the cementitious grout, resulting in less matrix cracking and shifting.

Considering that the internal reinforcing steel is treated as an elastic perfectly plastic material, neglecting the effect of strain hardening, the FSDT and HSDT results for midspan deflection under loads producing yielding are encouraging. With the exception of SRP-2, the predicted slope of the load—deflection curves after yielding is in good agreement with that obtained experi-

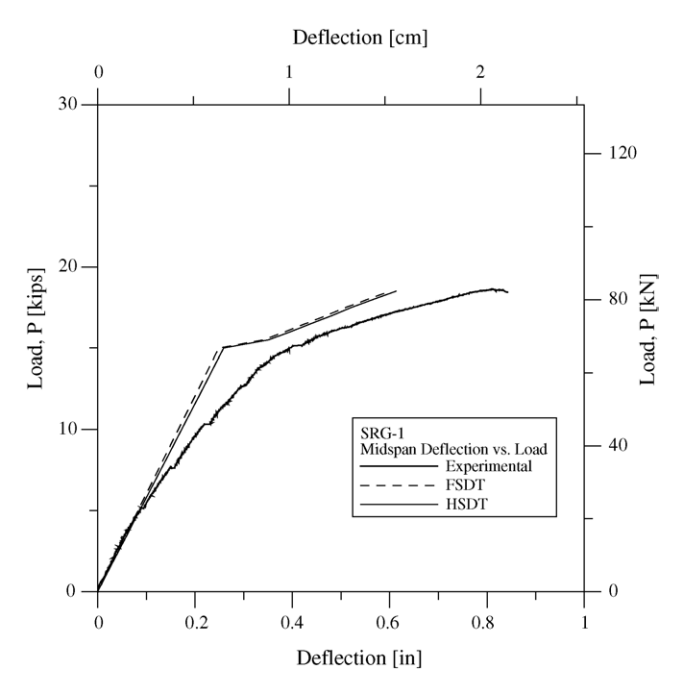


Fig. 9. Midspan deflection of SRG-1.

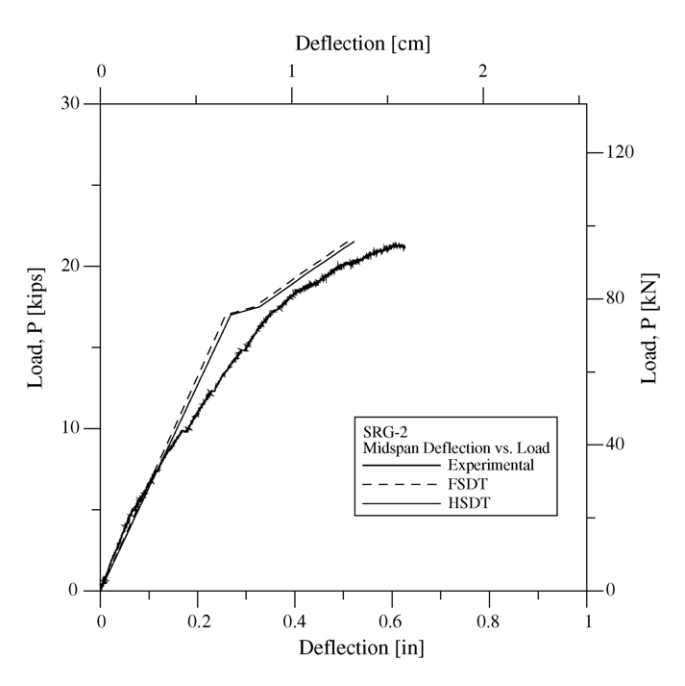


Fig. 10. Midspan deflection of SRG-2.

mentally. The ultimate load capacity of the RC beams could not be predicted by the two models since each of the four RC beams failed due to delamination of the SRP/SRG from the beam. Bond characterization studies are currently being conducted to account for this mode of failure.

5. Conclusions

Effective test methods were developed to determine the material properties of SRP/SRG lamina. The experimentally determined properties, summarized in Table 1, were employed in analytical models based on the FSDT and HSDT to predict the response of RC beams retrofitted with SRP/SRG and subject to four-point loading. Both the FSDT and HSDT models produced results that correlated well with experimental data for the midspan deflection of an RC beam reinforced with SRP or SRG. The models performed particularly well in the linear elastic regions of the beam deflection. When the effects of plasticity and cracking began to affect the response of the beams, they adequately predicted the general trend of the deflection.

Acknowledgements

The National Science Foundation (Grant #CMS-0301256) and Structural Preservation Systems funded this work. Hardwire LLC donated the steel tapes.

References

- [1] A. Ugural, Stresses in Plates and Shells, 2nd ed., McGraw-Hill, 1999.
- [2] J.M. Whitney, N.J. Pagano, J. Appl. Mech. (1970) 1031–1036.
- [3] J.N. Reddy, An Introduction to the Finite Element Method, 2nd ed., McGraw-Hill, 1993.
- [4] C.W. Bert, Compos. Struct. 2 (1984) 329-347.
- [5] J.N. Reddy, J. Appl. Mech. 51 (1984) 745-752.

- [6] Hardwire, LLC, What is Hardwire, Pocomoke City, MD, 2002, www.hardwirellc.com.
- [7] E. Wobbe, et al., Proceedings of the 2004 Symposium of the Society for the Advancement of Material and Process Engineering, Long Beach, CA, May 16–20, 2004, p. 20.
- [8] R.F. Gibson, Principles of Composite Material Mechanics, McGraw-Hill Inc., 1994.
- [9] G.A. Costello, Theory of Wire Rope, Springer-Verlag, New York, 1990.
- [10] C.K. Shield, G.A. Costello, J. Appl. Mech. 61 (1994) 1-8.